Applied Catalysis B: Environmental 179 (2015) 122–127

Contents lists available at ScienceDirect

Applied Catalysis B: Environmental

journal homepage: www.elsevier.com/locate/apcatb

Alumina coated nickel nanoparticles as a highly active catalyst for dry reforming of methane

Elham Baktash[a,d,*], Patrick Littlewood[b], Reinhard Schomäcker[b], Arne Thomas[a], Peter C. Stair[c,**]

[a] Functional Materials, Department of Chemistry, Technische Universität Berlin, Hardenbergstr. 40, 10623 Berlin, Germany
[b] Chemical Reaction Engineering, Department of Chemistry, Technische Universität Berlin, Straße des 17. Juni 124, 10623 Berlin, Germany
[c] Center for Catalysis and Surface Science, Department of Chemistry, Northwestern University, Evanston, IL 60208-3113, USA
[d] Chimie de la Matière Condensée de Paris, Sorbonne Universités, UPMC Univ Paris 06, CNRS, Collège de France, 11 Place Marcelin Berthelot, 75005 Paris, France

ARTICLE INFO

Article history:
Received 11 December 2014
Received in revised form 3 May 2015
Accepted 6 May 2015
Available online 7 May 2015

Keywords:
Dry reforming of methane (DRM)
Nickel oxide
Atomic layer deposition (ALD)
Nanoparticles
Core–shell structures

ABSTRACT

Alumina coated nickel nanoparticles were prepared employing atomic layer deposition (ALD) on nickel oxide (NiO) nanoparticles and subsequent reduction of the NiO core. The materials showed impressive activity and stability for dry reforming of methane at elevated temperatures (700–800 °C), especially when compared to the uncoated and reduced NiO nanoparticles. The stabilization against sintering at high temperatures is the crucial factor explaining the high catalytic activity of alumina coated Ni nanoparticles.

1. Introduction

Dry reforming is a process for syngas production from methane and carbon dioxide ($CH_4 + CO_2 \rightarrow 2H_2 + 2CO$). Syngas can be used for the production of numerous chemicals, including methanol, dimethyl ether, Fischer–Tropsch chemicals, ammonia, acetic acid, and formic acid [1–4]. Methane and carbon dioxide are two of the cheapest and most abundant carbon-containing materials. Furthermore, they are greenhouse gases; thus, their conversion into value added chemicals is of great interest. DRM is an endothermic reaction which even at higher temperatures needs suitable catalysts to observe sufficient conversions. Noble metals show high catalytic activity in dry reforming of methane (DRM) [5–9]; however, applying cheap and abundant metals such as Ni, which is also an active catalyst for this process, is certainly preferred [10]. However, Ni-based catalysts suffer from severe deactivation during the catalytic process [11]. Generally, catalyst deactivation is one of the major problems in heterogeneous catalysis. The time scale for deactivation can vary considerably depending on the operation conditions (temperature, pressure, reactants, etc.) type of catalyst and the reactor. Especially, in the case of endothermic processes, such as the DRM reaction, which require elevated temperatures for reasonable conversions, deactivation of catalysts is a serious problem. For Ni based catalysts in DRM, two major sources of deactivation have been identified, namely carbon deposition at lower (500–700 °C) and sintering at higher temperatures (700–800 °C) [10,12].

In order to decrease the cost of catalyst replacement and process shut down, tremendous efforts have been undertaken to improve catalyst stability in harsh conditions. Formations of alloys [13–17], partial passivation of the active sites with sulfur, tin or bismuth [14,15,18–20] are some examples of strategies employed for achieving this goal. Moreover, in order to avoid sintering which changes the active sites and accelerates coke formation, shells out of silica, [21,22] tin oxide [23] and zirconia [24] have been formed around the active catalysts by employing techniques such as chemical vapor deposition, dendrimer encapsulation or grafting. However, the formed shells often decreased the catalyst activity probably due to mass transfer limitation or active site coverage. Therefore, shell formation around active catalysts (also called

* Corresponding author at: Chimie de la Matière Condensée de Paris, Sorbonne Universités, UPMC Univ Paris 06, CNRS, Collège de France, 11 Place Marcelin Berthelot, 75005 Paris, France. Tel.: +33 0144 271544.
** Corresponding author. Tel.: +1 8474915266.
E-mail addresses: elham.baktash@upmc.fr (E. Baktash), pstair@northwestern.edu (P.C. Stair).

http://dx.doi.org/10.1016/j.apcatb.2015.05.018
0926-3373/

"inverse catalysts") [25–27] in a more controlled manner is necessary, to inhibit catalyst sintering but also maintain catalytic activity. Moreover, the preparation of inverse catalysts can give the opportunity to enhance selectivity of catalysts by partial coverage of catalytic active but unselective sites.

We report here on the preparation of alumina coated nickel-based catalysts from commercially available nickel oxide nanopowders. For conventional supported catalysts used in DRM, Al_2O_3 was considered to be an excellent support material due to its basicity, promoting a high conversion of CO_2 [28]. For the here presented inverse catalyst, Al_2O_3 coatings were prepared in a highly controlled manner using atomic layer deposition (ALD), by sequential exposures of NiO nanopowders to trimethyl aluminum (TMA) and water vapors. Different numbers of Al_2O_3 ALD cycles (5–20) were performed to generate protective layers of progressively increasing thickness on the NiO nanopowder. A pre-reduction of the Al_2O_3 covered NiO nanoparticles with hydrogen at 500 °C is carried out before the catalytic tests, yielding alumina coated Ni(0)-nanoparticles.

2. Experimental

2.1. Catalyst preparation

Ni oxide nanopowder (~50 nm particle size (TEM), 99.8% trace metals basis) was purchased from Sigma–Aldrich.

ALD was performed using a viscous flow reactor system similar to the one previously described [29] and a fixed-bed powder sample holder. Ultrahigh pure nitrogen (99.999%) was used as the carrier gas with a mass flow rate of 360 sccm. The system pressure was between 1 and 2 Torr. In traditional ALD, two precursors, A and B, are alternately dosed and purged through the reactor with the time sequence t_1–t_4. Here, A is trimethyl aluminum (TMA, Sigma–Aldrich, 97%); B is deionized water (H_2O); t_1 is the dose time for A; t_2 is the purge time for A; the t_3 is dose time for B; and t_4 is the purge time for B. The time sequence of 300–300–300–300 s was chosen for our system due to the porous nature of the NiO nanopowder which usually needs longer dosing and purging time than for flat substrates. [30] The over-coated samples were prepared using 5, 10, 15, and 20 cycles of Al_2O_3 ALD at 50 °C to generate the protective layers (NiO-*X*, *X*: number of alumina ALD).

2.2. Characterization

Nitrogen sorption isotherms were measured at liquid-nitrogen temperature (−196 °C) with an Autosorb-1. The samples were degassed at 120 °C overnight before the measurement. The Brunauer–Emmett–Teller (BET) surface area was calculated by multiple-point (five-point) measurement in the relative pressure range of 0.05–0.30.

The mass content of aluminium was measured by inductively coupled plasma optical emission spectroscopy (ICP-OES), Optina 2100 DV (PerkinElmer, USA).

Transmission electron microscopy (TEM) images were obtained on a FEI Tecnai G2 20 S-TWIN transmission electron microscope equipped with a LaB_6-source at 200 kV acceleration voltages, using amorphous carbon-coated copper grids. The specimens were dispersed in ethanol with ultrasonication and loaded onto a copper grid.

Temperature programmed oxidation (TPO) was carried out under 8 ml per min flow of 20% O_2 in He. The oxidation temperature was increased from room temperature to 800 °C with a heating ramp of 2 °C per minute. Outlet gas was analyzed using a quadrupole mass spectrometer (Inprocess Instruments GAM 200).

XRD was performed using a Bruker D8 Advance X-ray diffractometer with Cu Kα1 = 1.5418 Å radiation between 2° and 90° (2θ).

2.3. Catalytic testing

Catalyst testing was carried out in a fixed-bed quartz tube reactor (internal diameter 5 mm). The catalyst mass was diluted in quartz sand or glass balls with a total volume of 1.25 ml. The amount of catalyst used was typically 1 mg, although less was used for highly active catalysts in certain experiments to measure the catalytic activity away from thermodynamic equilibrium. The reactor was heated using an external furnace (HTM Reetz) controlled by a temperature probe within the catalyst bed. Each catalyst was reduced in-situ in pure H_2 for 1 h at 500 °C before testing; in-situ catalyst oxidation consisted of heating (20 K min^{-1}) and 1 h oxidation at 750 °C under 15 ml min^{-1} synthetic air flow. Typical reaction conditions were 30 or 60 ml min^{-1} reaction gas with composition CH_4:CO_2:He = 1:1:8 at atmospheric pressure. Outlet gases were analyzed (typically every 10 min) using an Agilent 7890A gas chromatograph equipped with thermal conductivity and flame ionization detectors.

3. Results and discussion

Al_2O_3 ALD performed using TMA and water is one of the most investigated and successful ALD procedures. [31–35] In this process:

1. TMA reacts with hydroxyl groups on the surface forming $Al(CH_3)_x$* (*surface species, x = 1–2) and CH_4.
2. Evacuation or purging with an inert gas like nitrogen removes the non-reacted reactants and the gaseous reaction by-products.
3. After the following H_2O exposure, the $Al(CH_3)_x$* transforms to $Al(OH)_x$* (x = 1–2) and releases CH_4.
4. After the formation of a monolayer on the substrate, excess precursors are purged by the inert gas.

The film growth occurs in a layer-by-layer fashion. These cycles are repeated until the target film thickness is achieved. Recently, ALD Al_2O_3 protective layers with precise thicknesses were utilized to inhibit the sintering of Pd NPs. The catalytic performance of the resulting material was tested in the methanol decomposition reaction [36]. The catalytic activity of the Al_2O_3 protected Pd NPs was maintained or even slightly enhanced up to a certain thickness. It has been shown that catalyst deactivation due to sintering or coke formation could be effectively prevented by alumina coating with a thickness of 8 nm [37]. The same process might be applicable for the protection of other supported/unsupported nanoparticles or porous materials with catalytic application in reactions perform at elevated temperatures.

5, 10, 15 and 20 cycles of alumina ALD were applied to NiO nanoparticles. XRD patterns of the nanoparticles before and after coating showed the typical pattern of the nickel oxide phase (Fig. S1). N_2 physisorption was performed on the uncoated and coated samples (Table 1). The BET measurements on the uncoated nanoparticles yield a surface area of 99.2 m^2 g^{-1}. After 5 cycles of alumina ALD, the surface area reduced to 51 m^2 g^{-1}. The decrease in surface area becomes more pronounced with increasing the number of alumina ALD cycles. This gradual decrease of surface area by increasing the ALD cycles could be a consequence of partial filling of the nanoparticle voids by alumina layers. The increasing aluminum content, measured by ICP elemental analysis (Table 1) furthermore proves the successful deposition of thicker alumina layers with increasing cycle number. The morphology of the Ni oxide nanoparticles before and after coating was studied by transmission electron

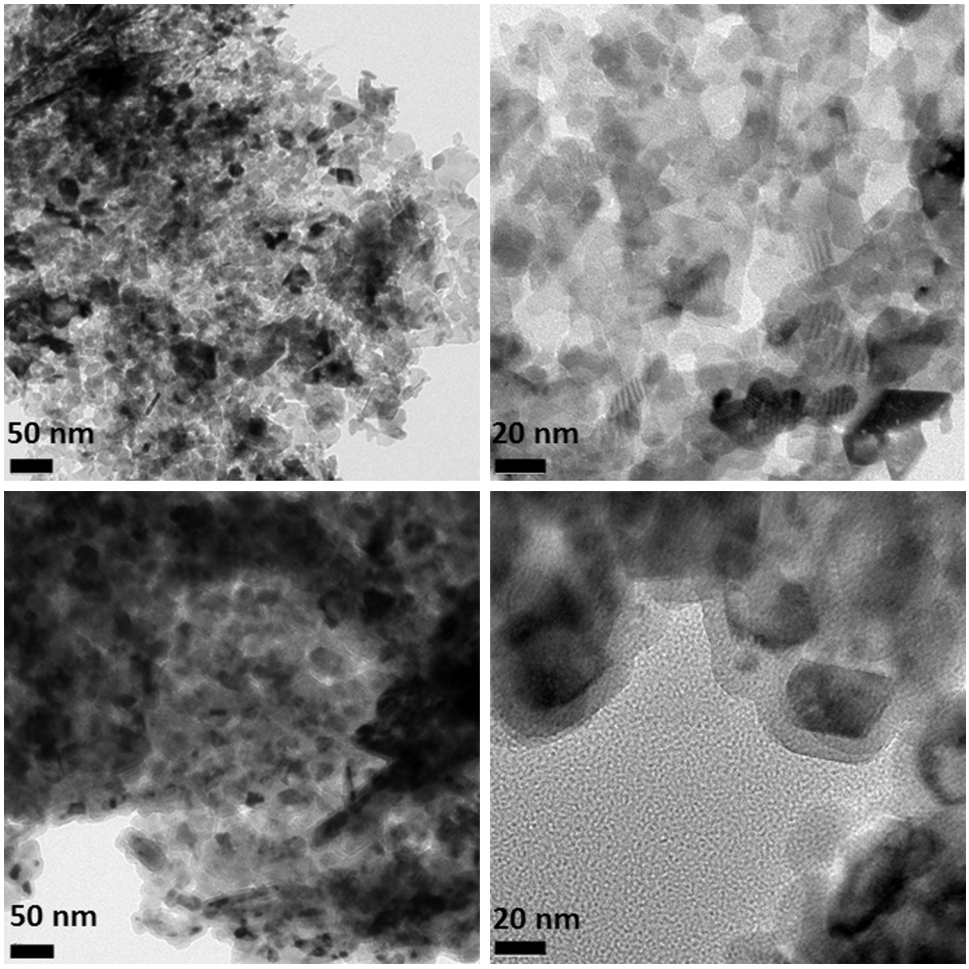

Fig. 1. TEM images of (a, b) uncoated NiO nanopowder, (c, d) coated with 20 cycles of alumina ALD (NiO-20).

microscopy (TEM). A homogeneous alumina coating on the NiO nanoparticles was observed after ALD (Fig. 1) with a thickness of around 8 nm for NiO-20 which has been covered by 20 cycles of alumina ALD (Fig. 2).

Each catalyst was reduced in-situ in pure H_2 for 1 h at 500 °C before testing, yielding reduction of NiO to Ni-nanopowders before the catalytic reaction. The XRD pattern of the uncoated oxide (NiO) shows complete reduction to nickel metal (Fig. S2), while for a coated sample (NiO-20) minor contributions of unreduced NiO can still be observed (Fig. S3). Note that for the sake of simplicity in the following the catalysts are termed NiO-*X*, even though it should be considered that in-situ reduction is needed to generate the catalytically active Ni(0) particles.

The uncoated NiO sample showed a sharp decrease in activity for the DRM already after 30 min time on stream and the conversion could afterwards not be increased by applying higher temperatures (Fig. 3). On the other hand, the NiO-5 sample coated with 5 cycles of alumina ALD) showed 26% CH_4 conversion at 500 °C in the beginning of the reaction, which however drops to

Table 1
Characterisation of the alumina coated NiO nanoparticles.

Name	Number of cycles	S_{BET}[a] ($m^2\ g^{-1}$)	Crystal phase[b]	Al (%)[c]
NiO	0	99.2	NiO	0
NiO-5	5	51	NiO	9.30
NiO-10	10	31.9	NiO	14.85
NiO-15	15	23.6	NiO	17.25
NiO-20	20	16.2	NiO	20.40

[a] Surface area of oxides ($m^2\ g^{-1}$).
[b] Crystalline phase as deduced from XRD patterns.
[c] Al (wt%) content based on ICP results.

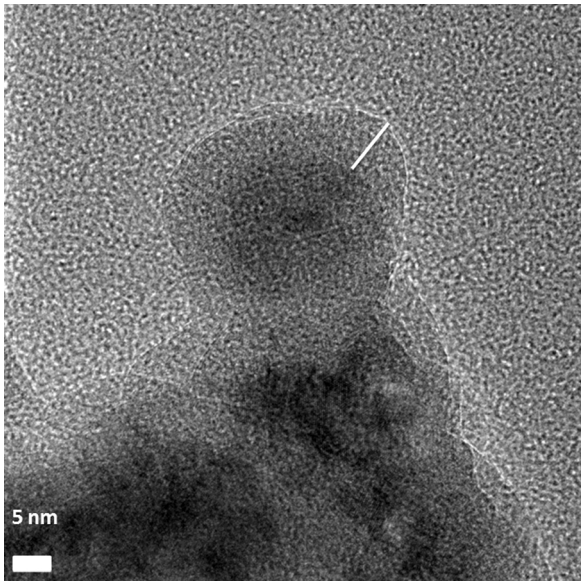

Fig. 2. HRTEM image of ALD-formed alumina coating on nickel oxide with the thickness of around 8 nm.

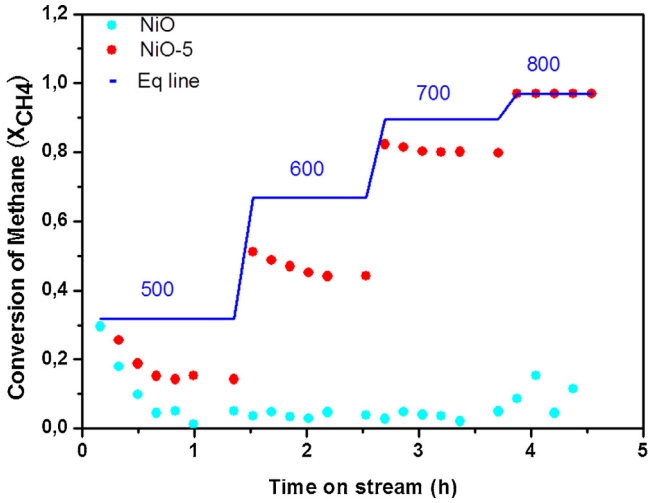

Fig. 3. CH_4 conversion over uncoated Ni nanopowder (20 mg Cat-Gas flow: 30 ml min^{-1}, GHSV: 90 Lh^{-1} g cat^{-1}) and alumina coated NiO-5 sample (1 mg Cat-Gas flow: 60 ml min^{-1}, GHSV: 3600 Lh^{-1} g cat^{-1}) at 500, 600, 700 and 800 °C.

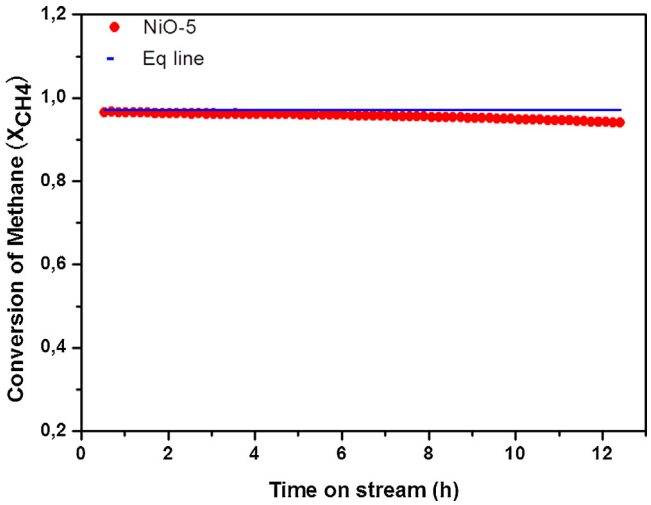

Fig. 5. CH_4 conversion over NiO-5 (0.55 mg Cat-Gas flow: 60 ml min^{-1}, GHSV: 6545 Lh^{-1} g cat^{-1}) at 800 °C.

15% after 1 h on stream. By increasing the reaction temperature to 600–700 °C, the methane conversion increased to 51–82%, respectively. The catalyst again showed some signs of deactivation at 600 °C but was almost stable at 700 °C. Notably, NiO-5 showed high methane conversion reaching the equilibrium conversion and good stability at 800 °C (Figs. 3 and S6). It should be noted that a direct comparison of the results for the uncoated and coated catalyst by weight is not possible, as to observe any conversion for the uncoated NiO a relatively high amount of 20 mg had to be used, while in the case of NiO-5 it was necessary to use less than 1 mg of catalyst at an undiluted flow of 60 ml min^{-1} to avoid thermodynamic equilibrium at higher temperatures.

To reveal the main source of NiO-5 deactivation at lower temperatures, as well as the reason for its high activity and stability at higher temperatures, long-term DRM reactions at 525 °C and 800 °C were carried out for this catalyst. Fig. 4 shows the result for the NiO-5 catalyst at 525 °C. A CH_4 conversion of 35% is observed at the beginning which drops to 20% during 12 h. Based on TPO (temperature programmed oxidation) measurements, 19.6 mg solid carbon (mostly graphite-like (Cγ), Fig. S7) was produced per mg catalyst suggesting that severe carbon deposition is the main reason for catalyst deactivation at lower temperatures. The DRM reaction at 800 °C was also performed for 12 h with NiO-5 as catalyst (Fig. 5).

It is observed that even with very low amounts of catalyst, and thus, high gas hour space velocity (0.55 mg cat, GHSV: 6545 Lh^{-1} g cat^{-1}) methane conversion reached the thermodynamic equilibrium of the DRM reaction at 800 °C. In this case, very low deactivation is observed after 12 h reaction time. It has been reported that the DRM reaction is accompanied by methane dissociation ($CH_4 \leftrightarrow C + 2H_2$) above 640 °C, possibly as part of the DRM reaction pathway. On the other hand, above 820 °C the reverse water gas shift reaction ($CO_2 + H_2 \leftrightarrow CO + H_2O$) and Boudouard reaction ($2CO \leftrightarrow C + CO_2$) do not occur. Methane dissociation and Boudouard reaction are, therefore, the reactions responsible for carbon deposition in the temperature range of 550–700 °C [38], while carbon deposition is decreased in the DRM reaction at temperatures higher than 700 °C. However, at these high temperatures, particle sintering is a major problem. Therefore, based on the catalytic results, it can be concluded that 5 cycles of alumina ALD can already protect the Ni particles from sintering at temperature as high as 800 °C. This protection results in high and stable methane conversions.

The methane conversions obtained using NiO-*X* catalysts prepared with different numbers of alumina ALD cycles are presented in Fig. 6. The catalyst prepared with 10 cycles, NiO-10, achieved lower methane conversion at 500, 600 and 700 °C but similar conversion at 800 °C compared to NiO-5, which is however limited

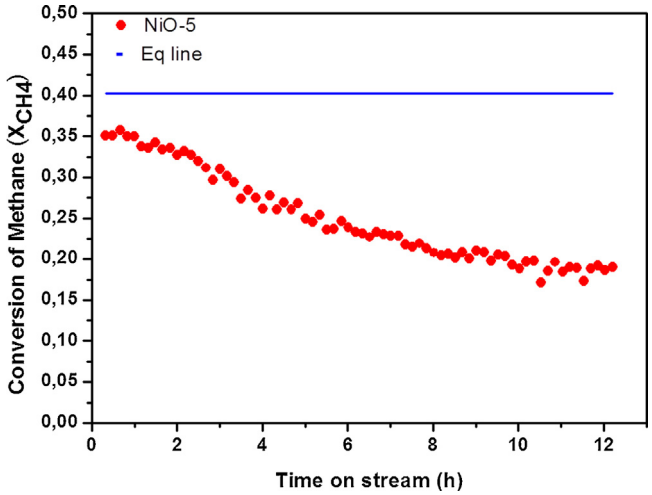

Fig. 4. CH_4 conversion over NiO-5 (1.94 mg Cat-Gas flow: 30 ml min^{-1}, GHSV: 928 Lh^{-1} g cat^{-1}) at 525 °C.

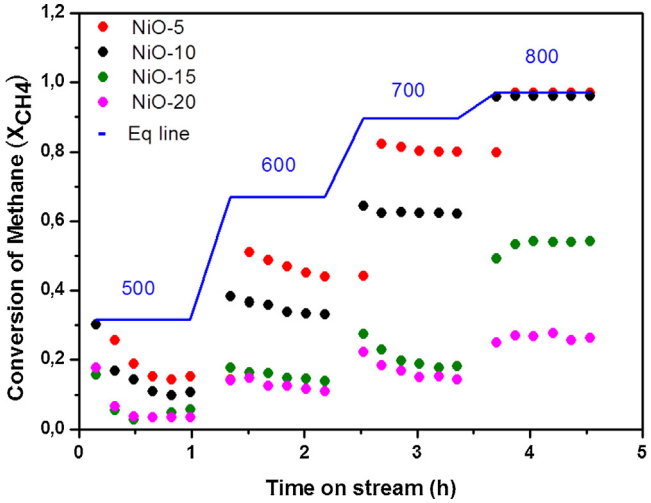

Fig. 6. CH_4 conversion over NiO-5, NiO-10, NiO-15 and NiO-20 at 500, 600, 700 and 800 °C,(1 mg Cat-Gas flow: 30 ml min^{-1}, GHSV: 3600 Lh^{-1} g cat^{-1}.

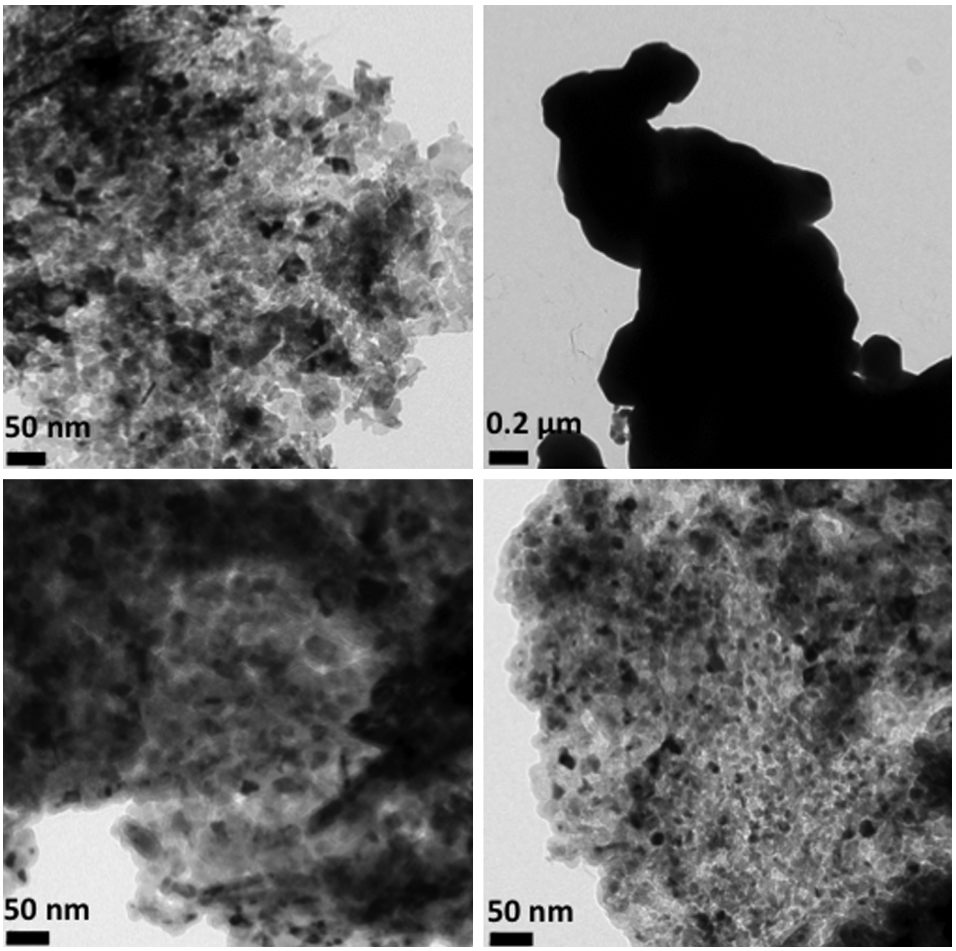

Fig. 7. TEM images of NiO, (a) before and (b) after reduction, NiO-5, (c) before and (d) after reduction.

by the thermodynamic equilibrium. A decreasing trend of activity is also observed for thicker alumina coatings, i.e. after 15 and 20 cycles, most probably due to mass transfer limitations (Table 2). All catalysts prepared by ALD showed outstanding activity in comparison to benchmark dry reforming catalysts. Table S1 summarizes activities of recently published Ni catalysts for DRM [39–51], several of which are described as highly active, indicating the high benefits to catalytic activity of the ALD synthesis route. The higher activity of NiO-5 compared to the catalysts of Gould et al. [39] (ALD with alumina supported Ni nanoparticles) can be attributed to a higher Ni: support ratio (rates per mole of Ni are the same order of magnitude), allowing for a majority Ni-nanoparticle catalyst.

The fact that the Ni surface is still accessible to the reactants even after 20 ALD cycles suggests that the Al_2O_3 coatings are porous. Experimental and theoretical (DFT calculations) studies showed that in the case of alumina coatings on Pd NPs with TMA, $-CH_3^*$ surface species formed after TMA deposition inhibit further TMA chemisorption. This inhibition results in discontinuities in the alumina film and introduces porosity [37,52–54]. The porosity of the ALD-formed alumina coating could be enhanced via high temperature treatment or prolonged reaction at elevated temperatures. Therefore, the nickel-based catalyst might be modified by modulating the porosity of the alumina coating. NiO-20 showed lower conversion at 525 °C compared to NiO-5; however, only 0.42 mg carbon per mg catalyst were produced during 12 h time on stream, showing that the alumina coating can also prevent carbon formation besides the protection against sintering (Figs. S4 and S5, Table S2).

From the catalytic activity trend, it can be seen that for Ni nanopowder, 5 cycles of alumina ALD is the optimum number of cycles to cover the catalyst and protect it from sintering at elevated temperatures, while maintaining the high catalytic activity. Fig. 7 proves this assumption showing the morphology changes of Ni nanopowders, with and without alumina coating after a reduction step under hydrogen while heating at 500 °C for 1 h (the pretreatment of the catalysts before DRM). While the particle size of alumina coated NiO remained almost unchanged, severe agglomeration and sintering occurred for the uncovered catalyst (NiO). This is also supported by the XRD measurements before and after reduction of NiO and NiO-20, respectively (Figs. S2 and S3). Using the Scherrer formula, an average crystallite size of 9.4 nm is observed for the uncoated NiO, which is largely increased to 34 nm

Table 2
Methane conversion rate in presence of NiO-*X* catalysts with different number of alumina ALD coating.

Catalyst	CH_4 conversion rate (mmol min^{-1} g cat^{-1})	CH4 conv. (%)	GHSV (Lg^{-1} h^{-1})	Temp. (°C)	CH_4/CO_2 ratio	yCH_4 in feed
NiO-20 ALD	41.9	17	3600	700	1–1	0.1
NiO-15 ALD	51.1	21	3600	700	1–1	0.1
NiO-10 ALD	153.8	63	3600	700	1–1	0.1
NiO-5 ALD	196.3	80	3600	700	1–1	0.1
NiO-5 (stable rate 50 h)	725.7	41	5143	800	1–1	0.5

for the Ni(0) particles after reduction, showing severe sintering. On the other hand, for NiO-20 particles, the crystallite size of the reduced and coated Ni(0) decreases to 8.4 nm due to the higher Ni(0) density.

NiO-5 was also tested at 800 °C with a high flowrate and undiluted equimolar DRM feed (Fig. S8). After a period of stabilization, the catalyst showed steady activity for 50 h at far below equilibrium conversions which could not be improved by oxidation-reduction, supporting the conclusion that the alumina coating stabilizes NiO against severe sintering and carbon deposition. This notably high residual activity during stable performance is listed in Table 2.

The stabilization against sintering at high temperature is a crucial factor which explains the high catalytic activity of alumina coated Ni nanopowder in comparison to the uncoated sample. This has also been proven via three runs of catalytic tests in presence of NiO-5 catalyst (Fig. S9). The activity is lower after the first run, but after burning off the carbon between the 2nd and 3rd runs, the activity is back to its original level. It confirms that the catalyst deactivates from coke deposition, but is extremely resistant to other forms of deactivation (most importantly, sintering). Also it has been shown in this work that at lower temperature (525 °C) the application of thicker alumina layers (20 cycles) can inhibit coke formation on the particle surface. Moreover, the alumina coatings may actively take part in the DRM reaction. Generally, two main mechanisms have been proposed for the dry reforming reaction. In the first mechanism, adsorption of CH_4, its dissociation into H_2 along with carbon species and adsorption of CO_2, all take place on the active metal sites. Then, carbon species formed from methane dissociation reacts with CO_2 to produce CO [3,55,56]. In the second mechanism, it has been proposed that CH_4 molecules adsorbed on active metal sites decompose to H_2 and CH_x species. CO_2 molecules adsorb to nearby metal oxide sites or the interface between metal site and the support, then dissociate into CO and surface oxygen or OH species. It has been shown that on a basic (alumina) or neutral support (zirconia) CO_2 is activated on the support, forming carbonate species. Then, the carbonate is reduced by CH_x molecules, forming active species that produce CO [57,58]. In the case of covered NiO materials, porous alumina layers may play the same role as in the conventional alumina-supported metal catalysts.

4. Conclusions

A series of alumina coated NiO nanopowders was prepared by employing alumina ALD with different numbers of cycles (5–20). The material prepared with 5 cycles of Al_2O_3 ALD showed significant enhancement in catalytic activity compared to uncoated catalyst at elevated temperatures (700–800 °C). The formation of alumina coating strongly inhibits catalyst sintering which is the main reason for the significant increase in activity and stability of the NiO-5 catalyst compared to uncoated NiO and other Ni-based catalysts.

Acknowledgments

Financial support from the Cluster of Excellence “Unifying Concepts in Catalysis” (UniCat) as well as Center for Catalysis and Surface Science of Northwestern University are gratefully acknowledged.

Appendix A. Supplementary data

Supplementary data associated with this article can be found, in the online version, at
http://dx.doi.org/10.1016/j.apcatb.2015.05.018

References

[1] M.A. Pen˜a, J.P. Gómez, J.L.G. Fierro, Appl. Catal. A – Gen. 144 (1996) 7.
[2] K. Aasberg-Petersen, J.-H. Bak Hansen, T. Christensen, I. Dybkjaer, P.S. Christensen, C. Stub Nielsen, S.E. Winter Madsen, J. Rostrup-Nielsen, Appl. Catal. A – Gen. 221 (2001) 379.
[3] J.R. Rostrup-Nielsen, Catal. Today 18 (1993) 305.
[4] J.H. Lunsford, Catal. Today 63 (2000) 165.
[5] A. Erdohelyi, J. Catal. 141 (1993) 287.
[6] Z. Zhang, J. Catal. 158 (1996) 51.
[7] C. Carrara, J. Múnera, E.A. Lombardo, L.M. Cornaglia, Top. Catal. 51 (2008) 98.
[8] P. Ferreira-Aparicio, C. Márquez-Alvarez, I. Rodríguez-Ramos, Y. Schuurman, A. Guerrero-Ruiz, C. Mirodatos, J. Catal. 184 (1999) 202.
[9] F. Barrai, T. Jackson, N. Whitemore, M. Castaldi, Catal. Today 129 (2007) 391.
[10] S. Wang, G. Lu, G. Millar, Energy Fuels 0624 (1996) 896.
[11] A.M. Gadalla, B. Bower, Chem. Eng. Sci. 43 (1988) 3049.
[12] L. Guczi, A. Erdôhelyi, Catalysis for Alternative Energy Generation, Springer, New York, 2012.
[13] J.R. Rostrup-Nielsen, I. Alstrup, Catal. Today 53 (1999) 311.
[14] D.L. Trimm, Catal. Today 49 (1999) 3.
[15] P. Biloen, J. Catal. 63 (1980) 112.
[16] N. Macleod, J.R. Fryer, D. Stirling, G. Webb, Catal. Today 46 (1998) 37.
[17] A.K. Rovik, S.K. Klitgaard, S. Dahl, C.H. Christensen, I. Chorkendorff, Appl. Catal. A – Gen. 358 (2009) 269.
[18] J. Radnik, A. Benhmid, V.N. Kalevaru, M.-M. Pohl, A. Martin, B. Lücke, U. Dingerdissen, Angew. Chem. Int. Ed. 44 (2005) 6771.
[19] D.T. Wickham, J. Engel, M.E. Karpuk, US Patent, US20020128161, November 19, 2002.
[20] K.K. Ghosh, D. Kunzru, Ind. Eng. Chem. Res. 27 (1988) 559.
[21] S.H. Joo, J.Y. Park, C.-K. Tsung, Y. Yamada, P. Yang, G.A. Somorjai, Nat. Mater. 8 (2009) 126.
[22] M. Seipenbusch, A. Binder, J. Phys. Chem. C 113 (2009) 20606.
[23] K. Yu, Z. Wu, Q. Zhao, B. Li, Y. Xie, J. Phys. Chem. C 112 (2008) 2244.
[24] P.M. Arnal, M. Comotti, F. Schüth, Angew. Chem. Int. Ed. 45 (2006) 8224.
[25] J.A. Rodríguez, J. Hrbek, Surf. Sci. 604 (2010) 241.
[26] J.A. Rodriguez, J. Graciani, J. Evans, J.B. Park, F. Yang, D. Stacchiola, S.D. Senanayake, S. Ma, M. Pérez, P. Liu, J.F. Sanz, J. Hrbek, Angew. Chem. Int. Ed. 48 (2009) 8047.
[27] D.V. Potapenko, J. Hrbek, R.M. Osgood, ACS Nano 2 (2008) 1353.
[28] J. Nakamura, K. Aikawa, K. Sato, T. Uchijima, Catal. Lett. 25 (1994) 265.
[29] J.W. Elam, M.D. Groner, S.M. George, Rev. Sci. Instrum. 73 (2002).
[30] J.A. Libera, J.W. Elam, M.J. Pellin, Thin Solid Films 516 (2008) 6158.
[31] M. Juppo, A. Rahtu, M. Ritala, M. Leskelä, Langmuir 16 (2000) 4034.
[32] A. Rahtu, T. Alaranta, M. Ritala, Langmuir 17 (2001) 6506.
[33] A.C. Dillon, A.W. Ott, J.D. Way, S.M. George, Surf. Sci. 322 (1995) 230.
[34] A.W. Ott, J.W. Klaus, J.M. Johnson, S.M. George, Thin Solid Films 292 (1997) 135.
[35] R.L. Puurunen, J. Appl. Phys. 97 (2005).
[36] H. Feng, J. Lu, P.C. Stair, J.W. Elam, Catal. Lett. 141 (2011) 512.
[37] J. Lu, B. Liu, J.P. Greeley, Z. Feng, J. a. Libera, Y. Lei, M.J. Bedzyk, P.C. Stair, J.W. Elam, Chem. Mater. 24 (2012) 2047.
[38] S. Wang, G.Q. (Max) Lu, G.J. Millar, Energy Fuels 10 (1996) 896.
[39] T.D. Gould, A. Izar, A.W. Weimer, J.L. Falconer, J.W. Medlin, ACS Catal. 4 (2014) 2714.
[40] J.F. Li, C. Xia, C.T. Au, B.S. Liu, Int. J. Hydrogen Energy 39 (2014) 10927.
[41] L. Xu, H. Song, L. Chou, Int. J. Hydrogen Energy 37 (2012) 18001.
[42] N. Wang, X. Yu, K. Shen, W. Chu, W. Qian, Int. J. Hydrogen Energy 38 (2013) 9718.
[43] N. Wang, X. Yu, Y. Wang, W. Chu, M. Liu, Catal. Today 212 (2013) 98.
[44] A. Serrano-Lotina, L. Daza, J. Power Sources 238 (2013) 81.
[45] A. Serrano-Lotina, A.J. Martin, M.A. Folgado, L. Daza, Int. J. Hydrogen Energy 37 (2012) 12342.
[46] M.H. Amin, K. Mantri, J. Newnham, J. Tardio, S.K. Bhargava, Appl. Catal. B Environ. 119–120 (2012) 217.
[47] Y.H. Guo, C. Xia, B.S. Liu, Chem. Eng. J. 237 (2014) 421.
[48] C. Xia, B. Liu, Y. Guo, Ind. Eng. Chem. Res. 53 (2014) 2189.
[49] J. Newnham, K. Mantri, M.H. Amin, J. Tardio, S.K. Bhargava, Int. J. Hydrogen Energy 37 (2012) 1454.
[50] K. Mette, S. Kühl, H. Düdder, K. Kähler, A. Tarasov, M. Muhler, M. Behrens, Chem. Cat. Chem. 6 (2014) 100.
[51] H. Düdder, K. Kähler, B. Krause, K. Mette, S. Kühl, M. Behrens, V. Scherer, M. Muhler, Catal. Sci. Technol. 4 (2014) 3317.
[52] N.A. Ray, R.P. Van Duyne, P.C. Stair, J. Phys. Chem. C 116 (2012) 7748.
[53] J. Lu, J.W. Elam, P.C. Stair, Acc. Chem. Res. 46 (2013) 1806.
[54] J. Lu, B. Fu, M.C. Kung, G. Xiao, J.W. Elam, H.H. Kung, P.C. Stair, Science 335 (2012) 1205.
[55] F. Solymosi, J. Mol. Catal. 65 (1991) 337.
[56] M. Mark, W. Maier, Angew. Chem. Int. Ed. (1994).
[57] J. Bitter, K. Seshan, J. Lercher, J. Catal. 286 (1997) 279.
[58] J. Nakamura, K. Aikawa, K. Sato, T. Uchijima, Catal. Lett. 25 (1994) 265.